

Knockout from ^{46}Ar : $\ell = 3$ neutron removal and deviations from eikonal theory

A. Gade,¹ D. Bazin,¹ C. A. Bertulani,^{2,*} B. A. Brown,^{1,2} C. M. Campbell,^{1,2} J. A. Church,^{1,2,†} D. C. Dinca,^{1,2} J. Enders,^{1,‡} T. Glasmacher,^{1,2} P. G. Hansen,^{1,2} Z. Hu,¹ K. W. Kemper,³ W. F. Mueller,¹ H. Olliver,^{1,2} B. C. Perry,^{1,2} L. A. Riley,⁴ B. T. Roeder,³ B. M. Sherrill,^{1,2} J. R. Terry,^{1,2} J. A. Tostevin,⁵ and K. L. Yurkewicz^{1,2}

¹National Superconducting Cyclotron Laboratory, Michigan State University, East Lansing, Michigan 48824

²Department of Physics and Astronomy, Michigan State University, East Lansing, Michigan 48824

³Department of Physics, Florida State University, Tallahassee, Florida 32306

⁴Department of Physics and Astronomy, Ursinus College, Collegeville, Pennsylvania 19426

⁵Department of Physics, School of Electronics and Physical Sciences, University of Surrey, Guildford, Surrey GU2 7XH, United Kingdom

(Received 1 December 2004; published 13 May 2005)

The $^9\text{Be}(^{46}\text{Ar}, ^{45}\text{Ar} + \gamma)X$ one-neutron removal reaction has been studied in inverse kinematics at 70 MeV/nucleon. Coincidences with γ rays served to disentangle knockout events leading to the ^{45}Ar ground state. The measured partial cross section corresponds to a spectroscopic factor of 4.9(7). The residue momentum distribution is compared with new calculations based on eikonal theory and represents the first case of an $\ell = 3$ neutron removal, as is expected for populating a $0f_{7/2}$ hole in the $N = 28$ projectile. However, the measured ^{45}Ar momentum distribution has a marked low-momentum tail suggestive of dissipative effects whereas the eikonal model predictions are symmetric. The angular distribution of the residues confirms that there is a deviation from the model.

DOI: 10.1103/PhysRevC.71.051301

PACS number(s): 24.50.+g, 21.10.Jx, 27.30.+t

Single-nucleon removal reactions, initiated by secondary beams of short-lived exotic nuclei, have large cross sections and are a powerful tool for studying the structure of light and medium-mass nuclei. In almost all cases, a large part of this cross section leads to excited states of the projectile residue. For this reason inclusive cross-section measurements are of very limited value. The measurement of coincidences between the reaction residue and its decay γ rays makes it possible to obtain partial cross sections. These serve two purposes: (i) Their absolute values allow spectroscopic factors to be deduced, and (ii) their differential cross sections, as a function of the residue parallel momentum, provide angular-momentum assignments, irrespective of their absolute normalization [1,2]. Both purposes are analogous to the use of low-energy transfer reactions for single-nucleon spectroscopy.

It has recently become evident that single-nucleon removal can provide information on absolute spectroscopic factors that test the extent to which the quasiparticles of effective-interaction theories correspond to physical reality. The recent work of Gade *et al.* [3] and the earlier papers cited therein agree with the results from $(e, e'p)$ reactions on stable nuclei, while also extending the spectroscopic possibilities to neutron removal and to unstable nuclei.

In this Rapid Communication we present the first instance of an $\ell = 3$ neutron-knockout cross section observed using an ^{46}Ar beam. The case is appealing because this $N = 28$ nucleus

is expected to have an almost full $0f_{7/2}$ neutron subshell and hence a large spectroscopic factor to the ^{45}Ar ground state. However, the relatively large neutron separation energy from its ground state, 5.45 MeV, allows transitions to many bound final levels and makes the reaction more challenging from an experimental point of view. Fortunately, the level scheme has been studied in fragmentation and β decay [4,5]. We will show that, although the contribution from excited states is of order 50% of the inclusive cross section, it is nevertheless possible to obtain the desired information on the ground-state partial cross section.

The ^{46}Ar secondary beam was obtained by fragmentation of a 110 MeV/nucleon ^{48}Ca primary beam provided by the Coupled Cyclotron Facility at the National Superconducting Cyclotron Laboratory (NSCL) at Michigan State University. The primary fragmentation target (1034 mg/cm² ^9Be) was located at the mid-acceptance target position of the large-acceptance A1900 fragment separator [6].

A secondary ^9Be target of 188(4) mg/cm² was placed at the target position of the high-resolution S800 magnetic spectrograph [7] and surrounded by the SeGA (segmented germanium array) γ array, configured with fifteen 32-fold segmented HPGe detectors [8]. These were arranged in two rings at a distance of 24 cm from the knockout target (to the center of the crystal) with central angles of 90° and 37° relative to the beam axis. The high degree of segmentation allowed for an accurate event-by-event Doppler reconstruction of the γ rays emitted by the reaction residues in flight. Details of the setup have been discussed elsewhere [9,10].

The average midtarget beam energy was 70 MeV/nucleon. The particle identification and the reconstruction of the momentum distribution of the ^{45}Ar residues was performed with the focal-plane detector system of the S800 spectrograph [7,11]. Information on the energy loss in the S800 ion chamber,

*Present address: Department of Physics, University of Arizona, Tucson, AZ 85721.

†Present address: Lawrence Livermore National Laboratory, Livermore, CA 94550.

‡Present address: Institut für Kernphysik, Technische Universität Darmstadt, Germany.

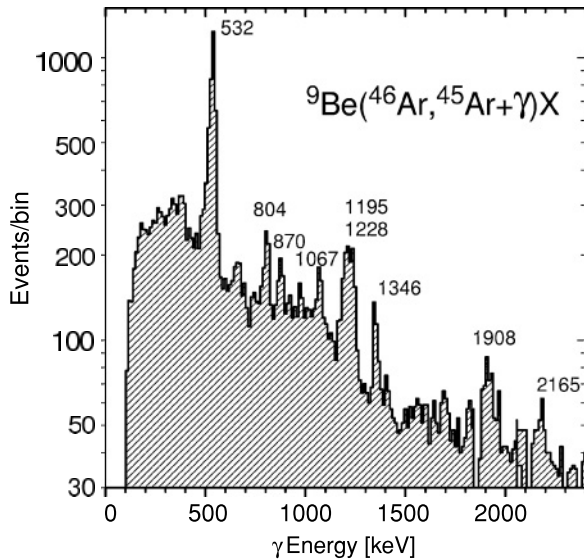


FIG. 1. Coincident γ rays referred to the rest system of the ^{45}Ar residues. Only peak structures that are clearly visible in the Doppler-reconstructed spectra of both rings of SeGA are attributed to the decay scheme of the knockout residue ^{45}Ar .

the time of flight (taken between scintillators), and the position and angles of the reaction products in the focal plane of the spectrograph were employed for event-by-event identification of the reaction residues.

The inclusive cross section σ_{inc} for one-neutron knockout to all bound ^{45}Ar final states was obtained from the yield of detected fragments relative to the number of incoming projectiles and the number density of the ^9Be secondary target. This analysis was performed repeatedly during the experiment to guard against fluctuations in the intensity of the incident beam. The main uncertainties stem from the choice of the software gates used for particle identification (7%), the correction for the momentum and angle acceptance of the S800 spectrograph (5%), and the stability of the beam (5%). These systematic errors are assumed to be independent and have been added in quadrature. The resulting inclusive cross section is $\sigma_{\text{inc}} = 122(13)$ mb.

Ten γ -ray transitions, observed in coincidence with the ^{45}Ar knockout residues, are shown in Fig. 1. The γ -ray detection efficiencies were determined from measurements with calibrated sources and from simulations that included the effect of the conversion of the observed γ response to a γ energy referred to the center-of-mass system. The efficiencies are estimated to be accurate to 5%. Although an anisotropic γ angular distribution is possible, from alignment effects in the knockout reaction, this is neglected in the evaluation of the γ intensities as the detector angles are very

close to the crossover points in the angular distributions and represent the average intensity (see, e.g., the example shown in Fig. 12 of Ref. [1]). The 532-keV line presents a special challenge because of its reported [4] half-life of $0.34^{+0.32}_{-0.15}$ ns. The corresponding mean flight path of several centimeters for the recoils affects the Doppler reconstruction (note the moderate asymmetry visible in Fig. 1) and, more importantly, increases the detection efficiency for the forward part of the array. We have therefore based our intensity for this γ -ray transition on the data taken at 90° , where the correction is small and where the large uncertainty in the half-life is of little importance.

The resulting energies and absolute intensities per ^{45}Ar fragment are 532(9) keV 32.0(40)%, 804(9) keV 4.8(9)%, 870(9) keV 2.8(6)%, 1067(11) keV 3.5(9)%, 1195(13) keV 9.1(13)%, 1228(13) keV 9.5(14)%, 1346(12) keV 4.4(9)%, 1403(14) keV $\leq 1.2\%$, 1908(6) keV 5.7(12)%, and 2165(18) keV 3.4(7)%. In the following we cite, for consistency, the energies measured in this work. More precise values can be found in the β decay of Ref. [5], where the γ -ray emission takes place at rest and therefore is not modified by the Doppler shift experienced in in-beam experiments. We interpret the intense 532-keV γ ray as depopulating the first excited $\frac{3}{2}^-$ state of ^{45}Ar . We do not have detailed information allowing a discussion of the placement of the γ rays of higher energy but draw on previous studies of ^{45}Ar from projectile fragmentation [4] and β decay [5]. Coincidence information, supported in our experiment, shows that the group of γ rays from 804(9) to 1228(13) keV feeds the first excited state, whereas the group of γ rays from 1346(12) to 2165(18) keV most likely decays to the ground state. An intensity balance based on this gives a branch of 47(5)% or 57(8) mb to levels above 1400 keV and a 3(3)% direct branch to the excited level at 532 keV. The branch to the ^{45}Ar ground state is 50(5)%, corresponding to a knockout cross section of 61(9) mb. The results for the two lowest levels are given in Table I.

The consistency of the analysis is supported by the very different shapes emerging for the momentum distributions shown in Figs. 2 and 3. They have been corrected for the acceptance of the S800 spectrograph. Data points with this correction exceeding a factor of 1.5 are excluded from the figures. In the analysis, the two position-sensitive cathode readout drift chambers (CRDCs) of the S800 focal-plane detector system and the magnetic settings of the spectrograph, in conjunction with the optics code COSY [12], permit a reconstruction of the longitudinal momentum of the residues on an event-by-event basis. The inclusive longitudinal momentum distribution is a superposition of the ground-state and excited-state contributions. The magnetic spectrograph was operated in the mode in which the beam is focused at the position of the reaction target in front of the S800 spectrograph.

TABLE I. Branching ratios b , cross sections, and spectroscopic factors for the lowest states of ^{45}Ar .

E_x (MeV)	I^π (\hbar)	nlj	b (%)	σ_{exp} (mb)	σ_{str} (mb)	σ_{dif} (mb)	$\sigma_{\text{exp}}/\sigma_{\text{sp}}$	C^2S SM
0.0	$7/2^-$	$0f_{7/2}$	50(5)	61(9)	9.55	2.89	4.9(7)	5.41
0.532	$3/2^-$	$1p_{3/2}$	3(3)	3.6(36)	12.69	4.80	0.2(2)	0.65

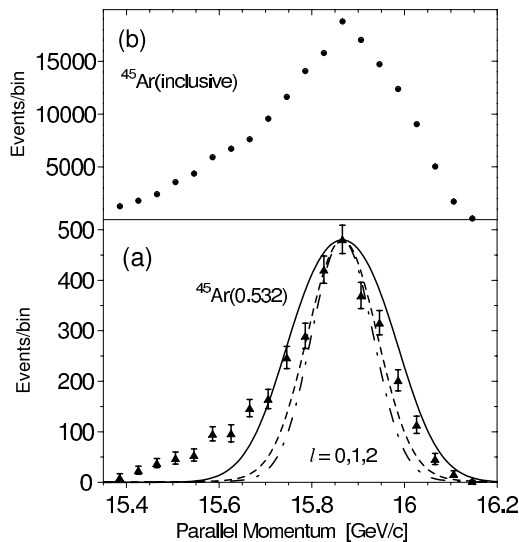


FIG. 2. (a) Experimental momentum distribution (black triangles) in coincidence with the 0.532-MeV γ ray. The contribution from γ rays of higher energy, determined from a gate set just above the peak, has been subtracted. The theoretical distributions [19] are shown for $\ell = 0$ (dot-dashed), $\ell = 1$ (dashed), and $\ell = 2$ (solid). They have been transformed to the laboratory system and folded with the momentum profile shown in Fig. 3. (b) Inclusive momentum distribution (black dots), shown on the same relative scale as the non coincident events in Fig. 3. The errors are smaller than the size of the points.

This offers a larger momentum bite, but at the cost of an inferior resolution to that using the “dispersion matched” optics setting. The momentum profile of the incoming ^{46}Ar beam provided the experimental resolution function shown in Fig. 3. The dashed line is a fit obtained by folding a square pulse with a Gaussian, thereby modeling the momentum bite of the spectrograph. The theoretical momentum distributions [19] were transformed to the laboratory frame and subsequently folded with the resolution function. Note that because of this correction, the $\ell = 0, 1$ shapes in Fig. 2(a) are very similar; the effect on the wide $\ell = 3$ distribution in Fig. 3(b) is small.

The momentum distribution in coincidence with the 532-keV γ ray is shown in Fig. 2. That in coincidence with the 1.2-MeV γ rays was identical and is not shown. These distributions must represent a superposition of components with different ℓ values. The calculation discussed in the following does not permit a precise theoretical fit to the shape, but the result is consistent with approximately equal contributions of $\ell = 0, 1$ and $\ell = 2, 3$. The momentum distribution of the cross section to the ground state of ^{45}Ar , shown in Fig. 3, was obtained by scaling the distribution in coincidence with the 0.532-MeV γ ray to 50% and subtracting it from the inclusive momentum spectrum. The conspicuous “tail” toward low momenta, which is one of the main results reported here, is not sensitive to the assumed relative intensity.

The theoretical analysis of the partial cross sections is similar to that of our previous work, as summarized in Ref. [1]. It assumes that the partial cross section for a given final

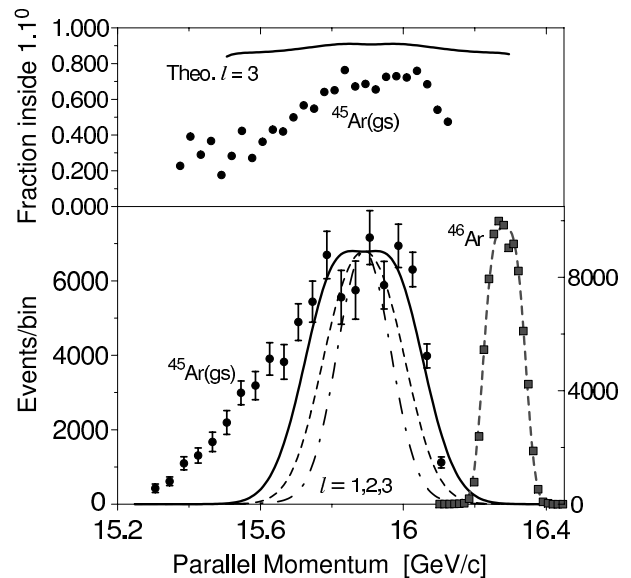


FIG. 3. The lower panel shows the measured momentum distribution of the unreacted ^{46}Ar fragments (black squares) and an analytical fit (dashed). The distribution of the ^{45}Ar ground state residues (black circles) obtained with a different field setting to exclude the unreacted ^{46}Ar beam particles is compared with theoretical calculations for $\ell = 1$ (dot-dashed), $\ell = 2$ (dashed), and $\ell = 3$ (solid). The upper panel shows the fraction of events at each momentum detected within 1.1° and a comparison (solid line) with a calculation based on eikonal theory.

state is

$$\sigma_{\text{th}} = R_s \left(\frac{A}{A-1} \right)^N C^2 S_j \sigma_{\text{sp}}, \quad (1)$$

where the A -dependent term is a center-of-mass correction valid for the N th oscillator shell and $C^2 S_j$ is the shell-model spectroscopic factor. The single-particle (unit) cross section σ_{sp} is based on a normalized single-nucleon wave function and hence a spectroscopic factor of unity [13,14]. It is the sum of contributions from stripping and diffraction dissociation detailed in Table I. Finally, the reduction factor R_s relative to the shell model takes into account couplings that go beyond the effective-interaction model space used for calculating $C^2 S_j$. For completeness we note that, for the ground-state cross section, the quantity R_s takes a value of 0.85(12), a result that we shall not discuss further.

As in previous work, the shell-model spectroscopic factors were calculated in a configuration-mixed model (see Brown [15]). The active space had the protons in the sd shell and the neutrons in the fp shell, with the interaction of Nummela *et al.* [16]. The assignments and spectroscopic factors for the lowest two states are given in Table I. The calculated energy of the $\frac{3}{2}^-$ state was 0.49 MeV, in good agreement with that measured. The shell model calculation gave two additional $\frac{7}{2}^-$ states at 2.40 and 2.70 MeV with spectroscopic factors of 0.26 and 0.99, respectively. Other negative-parity states were calculated to have spectroscopic factors smaller than 0.1. The negative-parity levels have not been identified experimentally and they would account for only a fraction of the cross section

to levels above 0.532 MeV. The main part of this cross section is almost certainly from fragmented positive-parity states from the *sd* neutron shell, not included in our model space. We note that the spectroscopic factor of 0.2(2) for the $p_{3/2}$ orbit is small and provides no indication for a breakdown of the $N = 28$ shell closure for ^{46}Ar .

For the calculation of the single-particle knockout partial cross sections there are several parameters, related to nuclear size, that have to be specified. In our most recent work [3] we have used self-consistent Hartree-Fock (HF) calculations based on the Skyrme-X parameter set [17]. These have been very successful in describing observables that reflect nuclear size (see [18]). The nucleon- ^{45}Ar relative motion wave function was calculated in a Woods-Saxon potential with the separation energy adjusted to the experimental value and with the rms radius of the orbital also taken from the HF calculation (with the appropriate center-of-mass correction [3]). For the $0f_{7/2}$ state these values are 8.02(4) MeV and 4.036 fm, respectively. The residue-target S matrix was constructed from the proton and neutron HF matter distributions for ^{45}Ar , as described in [3]. These lead to the values given in Table I. If we use instead just the HF matter radius, of 3.449 fm, and then assume Fermi-form matter distributions with diffuseness parameters of 0.5 or 0.6 fm, we obtain values 3% and 9% lower, respectively. These correspond to a theoretical error comparable to the experimental error.

The theoretical momentum distributions were calculated with a new method [19] that uses the same S matrices as were used for calculating the single-particle cross sections. Unlike the black-disk method used previously, the new method can also calculate the transverse momentum distribution. The distributions in coincidence with γ rays are presumably a mixture of components with $\ell = 0-3$, but the spectra lack the precision to enable a decomposition. The distribution to the ground state (Fig. 3) is in overall agreement with the calculation for $\ell = 3$, as expected for this state. It represents the first example of a distribution with angular momentum greater than 2.

The distribution for the $0f_{7/2}$ state in Fig. 3 shows an asymmetry with a “tail” toward lower momenta. A similar though less marked effect is present in Fig. 2 and has also been seen for $\ell = 0$ and 2 cross sections for the nuclei ^{34}Si [20] and ^{34}Ar [10]. Such an asymmetry implies effects that go beyond the eikonal approximation. The “transfer-to-the-continuum” model [21], which treats the residue-target collision semiclassically but the neutron transition amplitude quantum mechanically, leads in a natural way to asymmetric distributions. It accounts for some of the features in ^{34}Si , but it does not reproduce the tails seen there nor the more pronounced ones in the present work.

The asymmetry is reminiscent of the broadened and asymmetric parallel-momentum profile found for the halo nuclei ^{11}Be and ^{15}C , which could be understood by using a proper dynamical treatment of continuum-coupling effects in the diffractive channel [22]. However, the same explanation is unlikely to apply to this $0f_{7/2}$ state, which is strongly bound and for which diffractive breakup contributes only of order 25% of the cross section (see Table I). Instead, we require a modification to the stripping cross section. In the

calculations of Bertulani and Hansen [19] it emerged that in reactions of deeply bound states, the residue scatters elastically on the target simultaneously with the stripping. The elastic process transfers momentum from the residue to the target and so energy conservation will give rise to a low-energy tail. Estimates for a beryllium target, however, show that for the scattering angles of relevance, this effect is much too small to produce the momentum losses (of up to 500 MeV/ c) seen in Fig. 3. Multiple elastic collisions of the residue with the neutron and α particles produced by the impact of the stripped neutron with the target might lead to additional, dissipative momentum shifts, but for the moment this speculation is not supported by quantitative estimates.

We have further examined whether a deviation from eikonal theory is also visible in the angular distribution of the residues, as was the case for the diffractive breakup of ^{15}C [22]. The present experiment did not track the trajectory of the incoming ^{46}Ar projectile and therefore the angular resolution was limited to 0.5° full width at half maximum. As a semi-quantitative measure of the angular spread, we calculated the fraction of events falling inside 1.1° for each parallel-momentum setting (see Fig. 3). These fractions are considerably below the theoretical values calculated from the two-dimensional distribution [19] and, moreover, the deviation is greatest for the events away from the peak corresponding to larger momentum transfers. This lends qualitative support to the need for a dissipative mechanism acting in the final state of the reaction products.

One may wonder whether the observed deviations of the differential cross sections from eikonal theory could be a harbinger of a problem that would seriously affect the calculation of the total single-particle cross sections. We do not believe that this is the case as the two calculations are on quite different footings (see the original paper by Hencken, Bertsch, and Esbensen [23] on which [19] is based). In the eikonal treatment, the integrated partial cross sections are expressed by matrix elements with the structure of a sum rule and that involve only the overlap wave function of the transition. It expresses the joint probability that the nucleon is absorbed and that the residue undergoes, at most, elastic scattering. The expression, through completeness, is inclusive with respect to all final states. The analogous expression [23] for the differential cross section, in contrast, approximates the final states of the residue by plane waves, and hence their momentum distribution by a Fourier-like transform of the overlap function, modified by the absorptive terms. The calculation is therefore approximate in its description of the final states of the residue, target, and the absorbed nucleon.

We have presented the first case of a measured parallel-momentum distribution for $\ell = 3$ nucleon knockout. The deduced absolute spectroscopic factor, of 4.9(7), agrees with shell-model calculations for this nucleus with a valence shell dominated by the $\nu 0f_{7/2}$ state, and the low cross section to $\nu 1p_{3/2}$ state confirms that the $N = 28$ shell gap is well preserved, thus making ^{46}Ar a good semimagic nucleus. The parallel- and transverse-momentum distributions for this transition show interesting deviations from eikonal reaction theory, which are suggestive of missing

dissipative mechanisms. Similar but less pronounced effects have been observed in cross sections for $\ell = 0, 2$. The clarification of these deviations poses an interesting challenge.

We thank A. Stolz, T. Ginter, M. Steiner, and the NSCL cyclotron operations group for providing the high-quality

secondary and primary beams. We have appreciated discussions with A. Bonaccorso, A. G. Comacho, J.-L. Lecouey, O. Tarasov, and K. Yoneda. This work was supported by the National Science Foundation under Grants No. PHY-0110253, PHY-9875122, PHY-0244453, and PHY-0342281 and by the DOE Grant No. DE-FG02-04ER41338.

-
- [1] P. G. Hansen and J. A. Tostevin, *Annu. Rev. Nucl. Part. Sci.* **53**, 219 (2003).
- [2] P. G. Hansen and B. M. Sherrill, *Nucl. Phys.* **A693**, 133 (2001).
- [3] A. Gade *et al.*, *Phys. Rev. Lett.* **93**, 042501 (2004).
- [4] Zs. Dombradi *et al.*, *Nucl. Phys.* **A727**, 195 (2003).
- [5] J. Mrázek *et al.*, *Nucl. Phys.* **A734**, E65 (2004).
- [6] D. J. Morrissey, B. M. Sherrill, M. Steiner, A. Stolz, and I. Wiedenhöver, *Nucl. Instrum. Methods Phys. Res. B* **204**, 90 (2003).
- [7] D. Bazin, J. A. Caggiano, B. M. Sherrill, J. Yurkon, and A. F. Zeller, *Nucl. Instrum. Methods Phys. Res. B* **204**, 629 (2003).
- [8] W. F. Mueller, J. A. Church, T. Glasmacher, D. Gutknecht, G. Hackman, P. G. Hansen, Z. Hu, K. L. Miller, and P. Quirin, *Nucl. Instrum. Methods Phys. Res. A* **466**, 492 (2001).
- [9] A. Gade *et al.*, *Phys. Rev. C* **68**, 014302 (2003).
- [10] A. Gade *et al.*, *Phys. Rev. C* **69**, 034311 (2004).
- [11] J. Yurkon, D. Bazin, W. Benenson, D. J. Morrissey, B. M. Sherrill, D. Swan, and R. Swanson, *Nucl. Instrum. Methods Phys. Res. A* **422**, 291 (1999).
- [12] M. Berz, K. Joh, J. A. Nolen, B. M. Sherrill, and A. F. Zeller, *Phys. Rev. C* **47**, 537 (1993).
- [13] J. A. Tostevin, *J. Phys. G* **25**, 735 (1999).
- [14] J. A. Tostevin, *Nucl. Phys.* **A682**, 320c (2001).
- [15] B. A. Brown, *Prog. Part. Nucl. Phys.* **47**, 517 (2001).
- [16] S. Nummela *et al.*, *Phys. Rev. C* **63**, 044316 (2001).
- [17] B. A. Brown, *Phys. Rev. C* **58**, 220 (1998).
- [18] B. A. Brown, W. A. Richter, and R. Lindsay, *Phys. Lett.* **B483**, 49 (2000).
- [19] C. A. Bertulani and P. G. Hansen, *Phys. Rev. C* **70**, 034609 (2004).
- [20] J. Enders *et al.*, *Phys. Rev. C* **65**, 034318 (2002).
- [21] A. Bonaccorso, *Phys. Rev. C* **60**, 054604 (1999); A. Garcia-Camacho (private communication).
- [22] J. A. Tostevin, D. Bazin, B. A. Brown, T. Glasmacher, P. G. Hansen, V. Maddalena, A. Navin, and B. M. Sherrill, *Phys. Rev. C* **66**, 024607 (2002).
- [23] K. Hencken, G. Bertsch, and H. Esbensen, *Phys. Rev. C* **54**, 3043 (1996).